



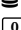
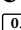
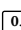
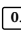
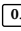
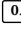
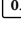
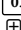
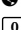
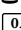
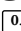
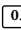
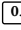
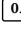
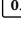
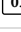
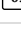
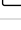







8.8%

Date: 2021-10-16 10:36 UTC

* All sources 73 | Internet sources 38 | Plagiarism Prevention Pool 14

- ✓ [21] www.researchgate.net/publication/248903777_Contact_Mapping_From_Gridded_Magnetic_Data-a_Comparison_of_Techniques
1.8% 25 matches
- ✓ [22] www.researchgate.net/publication/257517883_Sedimentation_and_inversion_history_of_three_molasse_basins_of_the_western_Central_Eastern_Des
0.5% 21 matches
- ✓ [23] docplayer.net/99117239-Geophysical-investigation-of-banded-iron-ore-mineralization-at-ero-north-central-nigeria.html
0.8% 20 matches
- ✓ [24] www.semanticscholar.org/paper/Integration-of-remote-sensing-and-aeromagnetic-data-Eldosouky-Abdelkareem/4e79e758854b87f26bc39260612f9fe
1.6% 15 matches
- ✓ [25] apet-eg.com/PDF/341A_P.10.pdf
0.6% 18 matches
- ✓ [26] moam.info/geophysical-investigation-of-banded-iron-ore_5c9493f7097c47356f8b464d.html
0.8% 18 matches
- ✓ [27] www.semanticscholar.org/paper/Syn-and-post-accretionary-structures-in-the-Central-Abdeen-Abdelghaffar/f36871eeb02667f1f63556c5061c891edc1
1.6% 10 matches
- ✓ [28] www.researchgate.net/publication/249863585_A_new_variable-magnetization_terrain_correction_method_for_aeromagnetic_data
0.5% 15 matches
- ✓ [29] www.researchgate.net/publication/341014606_Parana_Basin_As_Basement_In_The_Northern_Region_Of_The_Pelotas_Basin_Evidence_From_Seisn
0.0% 12 matches
- ✓ [30] www.researchgate.net/publication/257909770_Stress_analysis_and_tectonic_trends_of_southern_Sinai_Peninsula_using_potential_field_data_analysi
0.0% 12 matches
- ✓ [31] www.ias.ac.in/article/fulltext/jess/128/06/0156
0.0% 13 matches
- ✓ [32] www.sciencedirect.com/science/article/pii/S101836472100149X
1.1% 7 matches
- ✓ [33] ur.booksc.eu/book/75785293/e358e6
0.0% 12 matches
- ✓ [34] www.sciencedirect.com/science/article/abs/pii/S027311771930780X
0.7% 9 matches
- ✓ [35] www.sciencedirect.com/science/article/pii/S2090997717300937
0.8% 7 matches
- ✓ [36] www.researchgate.net/publication/340047829_Spatial-temporal_distribution_and_tectonic_setting_of_gold_deposits_in_the_Northern_margin_gold
0.5% 8 matches
- ✓ [37] crimsonpublishers.com/amms/pdf/AMMS.000556.pdf
0.0% 11 matches
- ✓ [38] www.researchgate.net/figure/Horizontal-gradient-magnitude-HGM-of-reduced-to-pole-high-resolution-aeromagnetic_fig3_258398919
0.0% 8 matches
- ✓ [39] www.sciencedirect.com/science/article/pii/S1018364721002470
0.5% 6 matches
- ✓ [40] www.researchgate.net/publication/330655754_A_methodology_for_three_dimensional_modeling_of_subsurface_geologic_structure_in_mantled_kar
0.0% 7 matches
- ✓ [41] www.cjees.ro/viewTopic.php?topicId=858
0.5% 5 matches
- ✓ [43] www.researchgate.net/publication/223815703_The_tectono-metamorphic_evolution_of_gneiss_complexes_in_the_Middle_Urals_Russia_A_reapprais
0.2% 5 matches
- ✓ [44] bu.edu.eg/portal/index.php?act=61
0.7% 2 matches
- ✓ [45] www.researchgate.net/publication/325188810_An_improved_stable_downward_continuation_of_potential_fields_using_a_truncated_Taylor_series
0.0% 6 matches
- ✓ [46] from a PlagScan document dated 2017-06-14 11:17
0.0% 3 matches

-
- ✓ [47]  pubs.geoscienceworld.org/jgs/article/148/1/83/93310/The-Kabus-ophiolitic-melange-Sudan-and-its-bearing
0.0% 4 matches
-
- ✓ [48]  from a PlagScan document dated 2020-08-19 16:05
0.0% 3 matches
-
- ✓ [49]  www.researchgate.net/figure/1st-Vertical-Derivative-of-the-magnetic-data-a-and-Satellite-imagery-of-the-study-area_fig3_308272487
0.0% 3 matches
-
- ✓ [50]  earth-planets-space.springeropen.com/articles/10.1186/BF03351853
0.5% 1 matches
-
- ✓ [51]  from a PlagScan document dated 2018-02-26 20:59
0.0% 3 matches
-
- ✓ [52]  www.researchgate.net/figure/The-vertical-derivative-of-the-total-magnetic-field-near-the-Corossil-structure-and-the_fig3_259553697
0.0% 3 matches
-
- ✓ [53]  cosparhq.cnes.fr/publications/
0.0% 2 matches
-
- ✓ [54]  from a PlagScan document dated 2020-12-31 18:09
0.0% 2 matches
-
- ✓ [55]  from a PlagScan document dated 2019-03-14 11:32
0.0% 2 matches
-
- ✓ [56]  from a PlagScan document dated 2018-12-12 08:06
0.0% 1 matches
-
- ✓ [57]  from a PlagScan document dated 2018-11-04 10:42
0.0% 1 matches
-
- ✓ [58]  from a PlagScan document dated 2018-10-17 07:11
0.0% 1 matches
⊕ 1 documents with identical matches
-
- ✓ [60]  pangea.stanford.edu/ERE/db/GeoConf/papers/SGW/2020/Perdana.pdf
0.0% 2 matches
-
- ✓ [61]  from a PlagScan document dated 2020-08-23 06:38
0.0% 1 matches
-
- ✓ [62]  from a PlagScan document dated 2021-05-03 09:26
0.0% 1 matches
-
- ✓ [63]  from a PlagScan document dated 2018-07-21 17:49
0.0% 1 matches
-
- ✓ [64]  books.openedition.org/cdf/5230?lang=en
0.0% 1 matches
-
- ✓ [65]  www.sciencedirect.com/science/article/pii/S1342937X19301509
0.0% 1 matches
-
- ✓ [66]  www.researchgate.net/figure/Depth-slices-of-seismic-amplitude-data-at-2-km-or-20-s-left-diagram-and-6-km-or-35-s_fig1_322037775
0.0% 1 matches
-
- ✓ [67]  from a PlagScan document dated 2018-10-18 10:02
0.0% 1 matches
-
- ✓ [68]  from a PlagScan document dated 2018-08-01 11:26
0.0% 1 matches
-
- ✓ [69]  from a PlagScan document dated 2018-05-08 20:13
0.0% 1 matches
-
- ✓ [70]  www.sintef.no/globalassets/project/geoscale/papers/spe119132-pa.pdf
0.0% 1 matches
-
- ✓ [71]  www.ncbi.nlm.nih.gov/pmc/articles/PMC2651473/
0.0% 1 matches
-
- ✓ [72]  www.researchgate.net/publication/269403698_Multiscale_Mimetic_Solvers_for_Efficient_Streamline_Simulation_of_Fractured_Reservoirs
0.0% 1 matches
-
- ✓ [73]  www.sciencedirect.com/science/article/pii/S1110982319303515
0.0% 1 matches
-
- ✓ [74]  link.springer.com/chapter/10.1007/978-1-4612-3788-4_20

16 pages, 3005 words

PlagLevel: 8.8% selected / 45.8% overall

167 matches from 75 sources, of which 59 are online sources.

Settings

Data policy: *Compare with web sources, Check against the Plagiarism Prevention Pool*

Sensitivity: *High*

Bibliography: *Bibliography excluded*

Citation detection: *Highlighting only*

Whitelist: --

Structural analysis and basement topography of Gabal Shilman area, South
Eastern Desert of Egypt, using aeromagnetic data

Abstract

The existing work deals with the structural analysis and detecting basement depth of G. Shilman area, South Eastern Desert (SED), Egypt. This work includes interpreting aeromagnetic data to map out structures within the study area and determine the depth of the magnetic basement which can be an aide to advance exploratory study. The first vertical derivative (1st VD) enhanced the short-wavelength and high-frequency features of the data. The analytic signal (AS) and horizontal gradient magnitude (HGM) maps well the structures of G. Shilman area.^[23] Statistical analysis of the delineated structures indicated that the NW, N_S, NNE and NE are the main structural trends controlling the study area. This suggests that the area was dominated by various stress regimes. The source parameter imaging (SPI) method which acts strongly at all magnetic latitudes was applied to the data to map the basement topography of G. Shilman area. The basement depths vary from about 0.1 km to about 1.5 km at the deepest part of the study area. The depth examination indicates that the recent deposits are not thick and reflect the shallow nature of the basement in G. Shilman area.

Key words: Aeromagnetic, First vertical derivative, AS, HGM, Spi.

1. Introduction

Magnetic method considers one of the common beneficial accessible tools that assist in the identification of the surface and subsurface geology. The goal of the utilization of the aeromagnetic analysis is to help in explaining the problems of

provincial geologic mapping and structure (Eldosouky, 2019; Sehsah et al., 2019; Eldosouky and Mohamed, 2021), representation of buried contacts, position of the presumable fields of rock differentiation, mineralization (Eldosouky et al., 2017, 2020a, 2021; Ekwok et al., 2019) and density of sedimentary cover. The magnetic enhancement has an interest that it is a quick and adequate technique for investigating the subsurface geologic structure and outlining the basement fractures (Ibraheem et al., 2018; Eldosouky et al., 2020b; Sehsah and Eldosouky, 2020; Pham et al., 2020, 2021).

Interpretation of magnetic data can be used to confirm the association between tectonics of and the structures within the sediments that overlying the basement. The linear features enhancement in potential field data is greatly helpful as it enables dykes, faults, and other features to be presented more obvious, thus assisting the geologic understanding process (Cooper, 2003).

In the present work, we apply 1st VD, AS, HGM, and SPI to RTP aeromagnetic data of G. Shilman area, SED, Egypt for well understanding of structural regimes and basement depth of the study area.

2. Geology of the study area

G. Shilman area situated to the southeast direction of Aswan in the south eastern desert (SED) of Egypt between latitudes of 22° 35' 00" and 22° 50' 00" N and longitudes of 33° 37' 50" and 33° 52' 50" E (Fig. 1). The Northern Sudan, Egyptian Eastern Desert (EED), and western part of Saudi Arabia have been collectively named the Arabian–Nubian Shield (ANS), which is distinguished by four principal rock associations: (i) an arc association; (ii) an ophiolite association; (iii) a gneiss association; and (iv) intrusions of granite (Abdel Rahman, 1995).

The foremost rock types in G. Shilman area are represented by ophiolites, syn-orogenic granodiorite, metasediments including marble, and metavolcanics (Fig. 1). The northwestern extension of the Allaqi-Heiani belt is defined by the ophiolitic rocks (Kröner et al., 1987). They are intruded by granodiorite and overlain by the arc metavolcanic–metasediment sequence. The ophiolites include completely talc-carbonates, serpentinitized peridotite, amphibolites and metagabbros (Abd El-Naby et al., 2000; Abdeen and Abdelghaffar, 2011). The most considerable serpentinite block occurs at G. Shilman producing a thrust nappe, which is also connected with a large metagabbro source. Older granites appear in the eastern part of G. Shilman area while younger granites occupy small portion at the northwestern part. Metavolcanic rocks are represented in the central part trending in the NW-SE direction. ^[22] Metasediments cover the most northwestern part of the study area with small traces to the east of metavolcanics (Abd El-Naby et al., 2000; Abdeen and Abdelghaffar, 2011) as shown in figure 1.

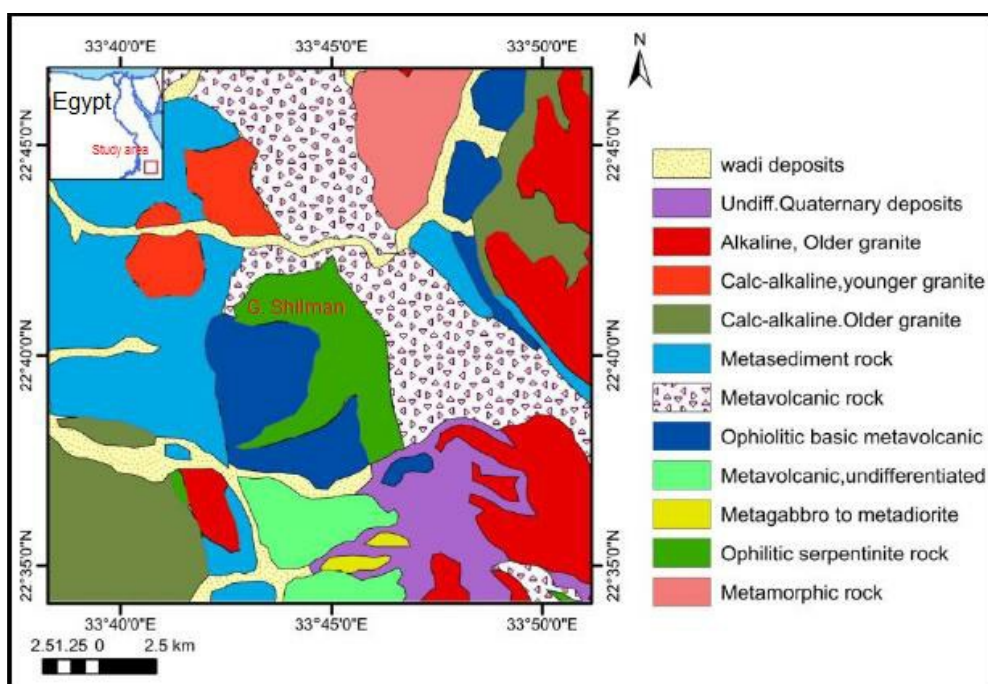


Figure 1. Location and geology of G. Shilman area.

Abd El-Naby et al. (2000) studied G. Shilman area and its surroundings and concluded that the study area revealed the remnants of back-arc oceanic crust, which causes a metamorphic sole underneath an allochthonous ultramafic source, which was overthrust as a hot body.

3. Data and Methodology

3.1. 1st vertical derivative (1st VD)

1st VD filter preferentially amplifies short-wavelength components of the data at the expense of longer wavelengths (Foss, 2011). 1st VD filter is commonly implemented to gridded data using FFT (Fast Fourier Transform) technique. Several VD of the magnetic domain can be estimated by multiplying the amplitude spectra of the field by a factor of the form:

$$VD = \frac{1}{n} [(u^2 + v^2)^{1/2}]^n \quad (1)$$

Where n = the vertical derivative order, (u, v) is the wavenumber corresponding to the (x, y) directions respectively. 1st VD is physically comparable to estimating the magnetic field concurrently at two points vertically overhead each other, subtracting the data and dividing the result by the vertical spatial separation of the measurement points. 1st VD has become nearly a basic requirement in magnetic enhancement projects. ^[21] This is derivative of the anomaly with respective of the depth of the body gives a better resolution of the anomaly itself. Calculation of the 1st VD in the aeromagnetic studies is equivalent to recognizing the vertical gradient directly with a magnetic gradiometer and has the same benefits, particularly enhancing near-surface sources,

overcoming deeper ones, and providing better resolution of closely-spaced sources (Foss, 2011).

3.2. Analytic signal (AS)

AS is a modern gradient technique, which is linked to magnetic fields by the derivatives. Roest et al.,^[21] (1992), explained that the amplitude of the AS can be determined from the three orthogonal derivatives of the magnetic data using the following expression:

$$A(x,y) = \sqrt{\left(\frac{\partial M}{\partial x}\right)^2 + \left(\frac{\partial M}{\partial y}\right)^2 + \left(\frac{\partial M}{\partial z}\right)^2} \quad (2)$$

Where $A(x,y)$ is the AS amplitude at (x,y) .

3.3. Horizontal gradient magnitude (HGM)

Horizontal gradient magnitude (HGM) approach (Blakely and Simpson, 1986; Nasreddine and Haydar, 2001)^[21] is conceivably the most simplistic method of determining the locations of magnetic contact and depths because it does not require the consideration of vertical derivatives but only the consideration of the two first-order horizontal derivatives of the domain. Thus, for a grid of magnetic field value $T(x, y)$, the HGM is expressed by:

$$HGM = \sqrt{\left(\frac{\partial f}{\partial x}\right)^2 + \left(\frac{\partial f}{\partial y}\right)^2} \quad (3)$$

3.4. Source parameter imaging (SPI) technique

Thurston and Smith (1997) developed the SPI method (SPI technique is called local wavenumber) because all the parameters that make up the body which include

susceptibility contrast, dip, and depth are computed from the complex AS. Fairhead et al. (2004) linked the source depth to the SPI (k) of the magnetic field which can be obtained from the computed HGM and VD of the RTP grid. The SPI method acts well at all magnetic latitudes which gives it the advantages for G. Shilman area. The SPI is given by:

$$k = \frac{\frac{\partial^2 M}{\partial x \partial z} \frac{\partial M}{\partial x} - \frac{\partial^2 M}{\partial x^2} \frac{\partial M}{\partial z}}{\left(\frac{\partial M}{\partial x}\right)^2 + \left(\frac{\partial M}{\partial z}\right)^2} \quad (4)$$

For the dipping contact, the K maxima are positioned directly overhead the contact edges and are independent of the remanent magnetization, strike, dip, declination and inclination of the magnetic data. The depth is determined at the edge of the source from the reciprocal of the SPI.

$$\text{Depth}(x = 0) = \frac{1}{K_{\max}} \quad (5)$$

4. Results and discussion

In our existing work, aeromagnetic data are employed to analyze the structural trends and basement topography of G. Shilman area. To perform this target, the reduced to the pole (RTP) map (Aero-Service, 1984) was enhanced (Fig. 2).

RTP map of the study area (Fig. 2) shows magnetic intensities (positive and negative anomalies) vary from -260 nT (Lows) to 250 (Highs) nT. It is clear to notice that the high magnetic values are related to ophiolitic serpentine and granites while low magnetic values are associated with metavolcanic and metasediment rocks.

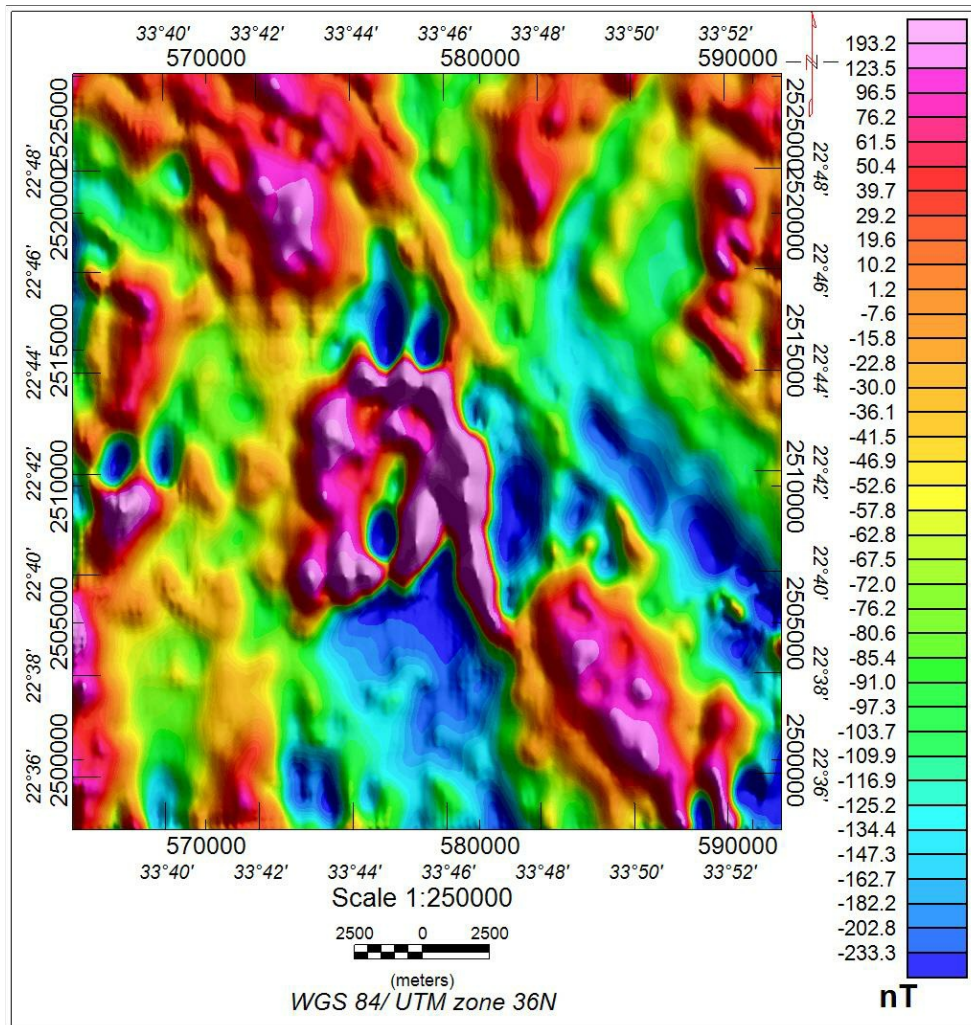


Figure 2. RTP map of G. Shilman area.

The first step of the structural analysis is to identify the high- and low-frequency elements of the data that are related to surface/subsurface geology. To enhance local features for outlining the edges of anomalous sources from the data, 1st VD map (Fig. 3a) was computed from the RTP grid. The 1st VD map shows that most of the local anomalies were in the N-S, NNE and NW directions.

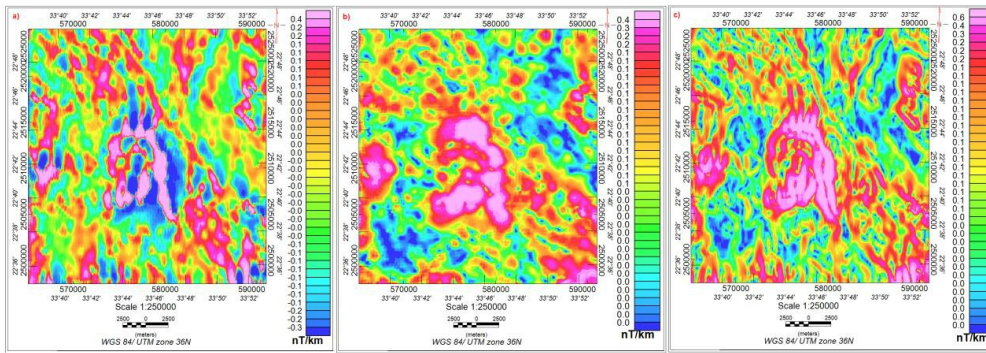


Figure 3. a) 1st vertical derivative; b) Analytic signal; and c) Horizontal gradient magnitude maps of G. Shilman area.

The AS map (Fig. 3b) emphasize the differences in the magnetization of the magnetic bodies in the study area and delineate discontinuities and anomalies texture. On the other hand, the HGM filter is applied to the RTP data to detect the contact locations of the bodies at depths as shown in Figure 3c.

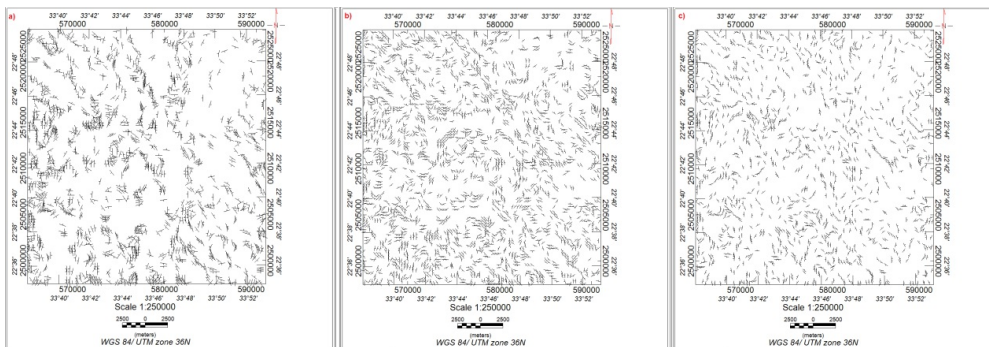


Figure 4. The structural lineament maps of the G. Shilman area derived from: a) 1st VD map (Fig.3a); b) AS map (Fig. 3b); and c) HGM map (Fig. 3c).

To distinguish the tectonic trends affecting G. Shilman area, the dominant magnetic structures on the 1st VD, AS and HGM maps (Figs. 3a, 3b and 3c) were traced and presented in the structural maps in figures (4a, 4b and 4c respectively) and statistically interpreted taking into record the azimuth and number of the structural

trends in each 10° and displayed in the form of rose diagrams (Figs. 5a, 5b and 5c) respectively.

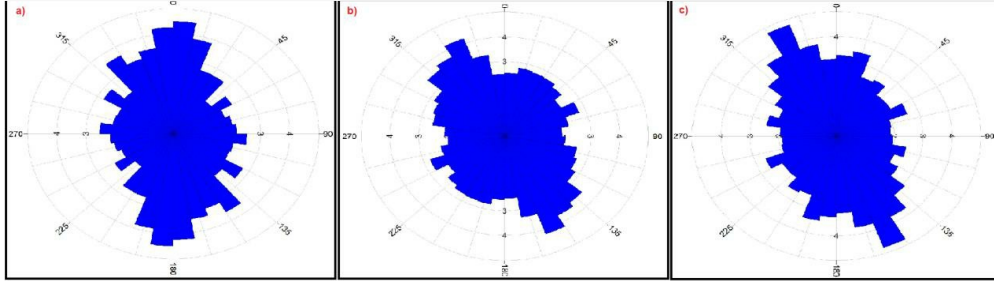


Figure 5. a) Lineament rose diagram of .1st VD map; b) Lineament rose diagram of .AS map; and c) Lineament rose diagram of .HGM map.

Lineaments that describe fracture/fault zones of G. Shilman area (Figs. 4a and 5a) from 1st VD revealed that the N-S, NW and NNE directions are the main structural trends controlling the shallow and local sources while the NW, NE, N-S, and ENE directions are the dominant ones revealed from the AS maps (Figs. 4b and 5b) and HGM maps (Figs. 4c and 5c). This indicates that the structural regime affecting the study area causing the N-S direction is the most recent while the NW direction the predominant structural tectonic trend at G. Shilman area (Eldosouky and Elkhateeb, 2018).

According to Zoheir and Klemm (2007), Zoher et al. (2017) and Elkhateeb et al.,^[36] 2021, the deformation history of the central part of the Allaqi-Heiani suture indicated that there is an intense crustal shortening that took place throughout the collision of east and west Gondwana (640–550 Ma). As a result, the Allaqi-Heiani suture was deformed by the post-accretionary N–S trending Hamisana Zone and related NW–SE sinistral and NE–SW dextral transpressional faults, during the Late Pan-African Najd orogen (e.g., Abdeen and Abdelghaffar, 2011).

The SPI depth map of G. Shilman area (Fig. 6) derived from the RTP data (Fig. 2) shows depth ranges from 0.1 km to about 1.5 km. The light to deep blue colors with depth ranges from 0.1 to 0.271 km show regions of shallow lying magnetic bodies. Red to pink colors with depth ranges from 0.6 to 1.4 km show areas of thicker sediments or deep-lying magnetic sources. SPI map (Fig. 6) maps basement topography well in G. Shelman area.

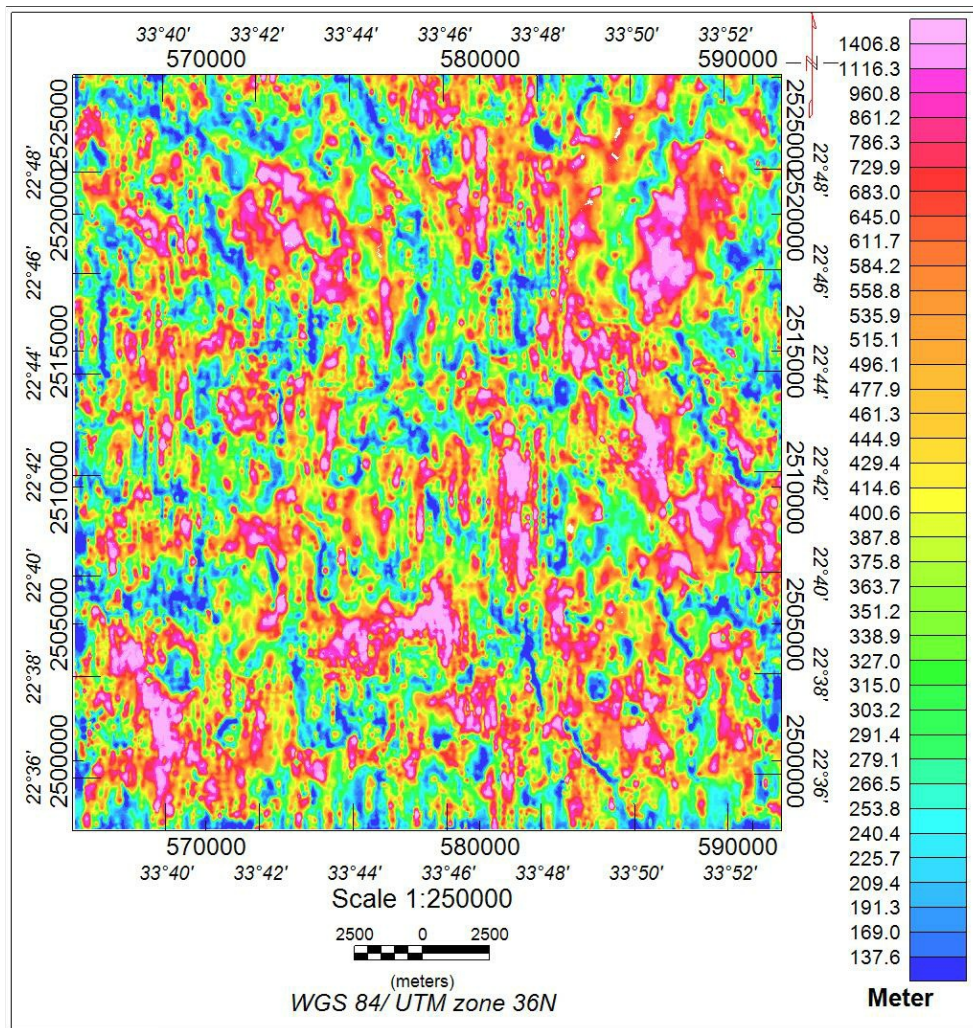


Figure 6. Source parameter imaging depth map of G. Shilman area.

5. Conclusion

The existing work deals with the analysis and interpretation of structural trends and mapping the basement topography of G. Shilman area, SED of Egypt, using aeromagnetic data. A variety of enhancement techniques were applied to RTP data of G. Shilman area. 1st vd, AS and HGM were applied to analyze the structural trends while SPI technique was applied to map basement topography.

^[25] 1st VD map of the study area outlined the structural features related to local sources (short-wavelength components) and illustrated that the N-S, NW and NNE directions were the most tectonic trends controlling the study area. Moreover, the 1st VD mapped well the edges of shallow sources. AS and HGM maps delineated the tectonic structural trends that controlling G. Shilman area. Structural and statistical analysis of these maps represented that the NW, NE, N-S and NNE directions were the most structural trends and the NW direction was predominant. Furthermore, HGM delineated edges of the magnetic sources more obviously than the edges which were represented by AS. The SPI depth map of the study area showed depths varied from 0.1 to about 1.5 km. ^[22] The applied enhancement techniques in the present work can be employed in alike rugged areas in the Egyptian Eastern Desert and other similar parts of the world for the structural analysis and depth estimation purposes.

Acknowledgements

This research was supported by Researchers Supporting Project number (RSP-2021/249), King Saud University, Riyadh, Saudi Arabia.

References

Abdeen, M. M, and Abdelghaffar, A. A., (2011)^[27]: **Syn- and postaccretionary structures in the Neoproterozoic Central Allaqi-Heiani suture zone, Southeastern Egypt.** Precambrian Research, 185, 95-108.

Abd El-Naby, H., Frisch, W., and Hegner, E., (2000): Evolution of the Pan-African Wadi Haimur metamorphic sole, Eastern Desert, Egypt. J. metamorphic Geol., 18, 639–651.

Abdel Rahman, A. M., (1995): Tectonic-magmatic stages of shield evolution: the Pan-African belt of northeastern Egypt. Tectonophysics, 242, 223–240.

Aeroservice Co. (1984): Final operational report of airborne Magnetic /radiation Survey in the Eastern Desert, Egypt. Aeroservice for EGPC, Houston, Texas, April 1984. Six volumes. An internal report. No.3609.

Blakely, R.J., and Simpson, R.W., (1986)^[21]: **Approximating edges of source bodies from magnetic and gravity anomalies.** Geophysics 51 (7), 1494–1498 (July).

Cooper, G.R.J., (2003): Feature detection using sun shading. Computers & Geosciences 29, 941–948.

Ekwok, S.E., Akpan, A.E., and Ebong, D. E., (2019): Enhancement and modeling of aeromagnetic data of some inland basins, southeastern Nigeria. Journal of African Earth Sciences, 155, 43-53.

Eldosouky, A.M., Abdelkareem, M., and Elkhateeb, S.O., (2017)^[24]: **Integration of remote sensing and aeromagnetic data for mapping structural features and hydrothermal**

alteration zones in Wadi Allaqi area, South Eastern Desert of Egypt. *Journal of African Earth Sciences*, doi: 10.1016.

Eldosouky, A.M., and Elkhateeb, S. O., (2018)^[35]: **Texture analysis of aeromagnetic data for enhancing geologic features using co-occurrence matrices in Elallaqi area, South Eastern Desert of Egypt.** *NRIAG Journal of Astronomy and Geophysics*, 7, 155–161.

Eldosouky, A.M., 2019. Aeromagnetic data for mapping geologic contacts at Samr El-Qaa area, North Eastern Desert, Egypt. *Arab J Geosci* 12, 2. <https://doi.org/10.1007/s12517-018-4182-2>.

Eldosouky, A. M., Sehsah, H., Elkhateeb, S. O., and Pour, A. B., (2020a)^[24]: **Integrating aeromagnetic data and Landsat-8 imagery for detection of post-accretionary shear zones controlling hydrothermal alterations: The Allaqi-Heiani Suture zone, South Eastern Desert, Egypt.** *Advances in Space Research* 65, 1008–024.

Eldosouky, A.M., Elkhateeb, S.O., Ali, A., Kharbish, S. (2020b)^[32]: **Enhancing linear features in aeromagnetic data using directional horizontal gradient at Wadi Haimur area, South Eastern Desert, Egypt.** *Carpathian J. Earth Environ. Sci.* 15(2):323–326. <https://doi.org/10.26471/Cjees/2020/015/132>.

Eldosouky, AM, Mohamed, H, 2021. Edge detection of aeromagnetic data as effective tools for structural imaging at Shilman area, South Eastern Desert, Egypt. *Arab J Geosci* 14, 13, <https://doi.org/10.1007/s12517-020-06251-4>

Eldosouky, A.M., El-Qassas, R.A.Y., Pour, A.B., Mohamed, H., Sekandari, M. (2021). Integration of ASTER satellite imagery and 3D inversion of aeromagnetic data for deep mineral exploration. *Advances in Space Research*, Volume 68, Issue 9, Pages 3641-3662, ISSN 0273-1177, <https://doi.org/10.1016/j.asr.2021.07.016>.

Elkhateeb, S.O., Eldosouky, A.M., Khalifa, M.O., and Aboalhassan, M., 2021. Probability of mineral occurrence in the Southeast of Aswan area, Egypt, from the analysis of aeromagnetic data. *Arab J Geosci* 14, 1514. <https://doi.org/10.1007/s12517-021-07997-1>.

Fairhaed, J. D., Green, C. M., Verduzco, B., and Mackenzie, C., (2004): A new set of magnetic field derivatives for mapping mineral prospects. 17th ASEG Geophysical Conference and Exhibition, Sydney, Australia, Expanded Abstract.

Foss, C., (2011): Magnetic data Enhancement and Depth Estimation. (H. Gupta, Ed.) *Encyclopedia of Earth Sciences Series*, 736-746.

Grauch, V. J. S., (1987)^[50]: **A new variable-magnetization terrain correction method for aeromagnetic data, *Geophysics* 52, 94–107.**

Ibraheem, I. M., Elawadi, E. A., and El-Qady, G. M., (2018): Structural interpretation of aeromagnetic data for the Wadi El Natrun area, northwestern desert, Egypt. *Journal of African Earth Sciences*, 139, 14-25.

Kröner, A., Greiling, R., Reischmann, T., Hussein, I. M., Stern, R. J., Kruger, J., Durr, S., and Zimmer, M., (1987): Pan-African Crustal Evolution in the Nubian segment of Northeast Africa. In: Kröner, A. (ed.). *Proterozoic Lithosphere Evolution*. Washington D.C., American Geophysical Union, 235-257.

Nassreddine, B., and Haydar, A. B., (2001): Interpretation of magnetic anomalies using the horizontal gradient analytical signal. *Annali Di Geofisica*, v. 44, pp. 505-526.

Pham, L.T., Oksum, E., Do, T.D., Nguyen, D.V., Eldosouky, A.M. (2021)^[32]. **On the performance of phase-based filters for enhancing lateral boundaries of magnetic and**

gravity sources: a case study of the Seattle uplift. *Arab J Geosci* 14, 129 (2021).
<https://doi.org/10.1007/s12517-021-06511-x>.

Pham, L.T., Eldosouky, A.M., Melouah, O., Abdelrahman, K., Alzahrani, H., Oliveira, S.P., Andráš, P. (2021). Mapping subsurface structural lineaments using the edge filters of gravity data. *Journal of King Saud University - Science*, Volume 33, Issue 8, 101594, ISSN 1018-3647, <https://doi.org/10.1016/j.jksus.2021.101594>.

Roest, W., Verhoef, J., & Pilkington, M., (1992): Magnetic interpretation using 3-D analytical signal. *Geophysics*, 57, 116- 125.

Searle, M., and Cox, J., (1999): Tectonic setting, origin, and obduction of the Oman ophiolite. *Geological Society of America Bulletin*, 111, 104–122.

Sehsah, H., Eldosouky, A. M., and El Afandy, A. H., (2019)^[27]► **Unpaired ophiolite belts in the Neoproterozoic Allaqi-Heiani Suture, the Arabian-Nubian Shield: Evidences from magnetic data.** *Journal of African Earth Sciences* 156 (2019) 26–34.
<https://doi.org/10.1016/j.jafrearsci.2019.05.002>.

Sehsah, H., & Eldosouky, A.M. (2020). Neoproterozoic hybrid forearc – MOR ophiolite belts in the northern Arabian-Nubian Shield: no evidence for back-arc tectonic setting, *International Geology Review*.
<https://doi.org/10.1080/00206814.2020.1836523>.

Thurston, J. B., and Smith, R. S., (1997)^[21]► **Automatic conversion of magnetic data to depth, dip, and susceptibility contrast using the SPI (TM) method:** *Geophysics*, 62, 807-813.

Zoheir, B.A., Klemm, D.D., 2007.^[44] [The tectono-metamorphic evolution of the central part of the Neoproterozoic Allaqi-Heiani suture, south Eastern Desert of Egypt.](#) *Gondwana Res.* 12, 289–304.

Zoheir, B., Emam, A., El-Amawy, M., Abu-Alam, T., 2017. Auriferous shear zones in the central Allaqi-Heiani belt: Orogenic gold in postaccretionary structures, SE Egypt. *J. Afr. Earth Sc.* <https://doi.org/10.1016/j.jafrearsci.2017.10.017>.